PrimPol-dependent single-stranded gap formation mediates homologous recombination at bulky DNA adducts

Ann Liza Piberger[1], Akhil Bowry[1]*, Richard D W Kelly[1]*, Alexandra K Walker[1], Daniel Gonzalez[2], Laura J Bailey[3], Aidan J Doherty[3], Juan Méndez[2], Joanna R Morris[1], Helen E Bryant[4], Eva Petermann[1]

[1]Institute of Cancer and Genomic Sciences, College of Medical and Dental Sciences, University of Birmingham, Birmingham B15 2TT, United Kingdom

[2] Molecular Oncology Program, Spanish National Cancer Research Centre, Madrid, Spain

[3]Genome Damage and Stability Centre, School of Life Sciences, University of Sussex, Falmer, Brighton BN1 9RQ, United Kingdom

[4]Department of Oncology & Metabolism, The Medical School, University of Sheffield, Sheffield S10 2RX, United Kingdom

Corresponding authors: A.L.Piberger@bham.ac.uk; E.Petermann@bham.ac.uk

*These authors contributed equally

Running title: Re-priming-mediated recombination

Abstract

Obstacles on the DNA template can lead to DNA replication fork stalling and genomic rearrangements. RAD51-mediated homologous recombination (HR) can promote restart and repair of stalled forks, but also post-replicative repair once the obstacle has been bypassed. Bulky DNA adducts are important replication-blocking lesions induced by environmental carcinogens, but it is not known whether they activate HR directly at stalled forks, or at gaps left behind ongoing forks. Here we show that in mammalian cells, bulky adducts predominantly induce HR at post-replicative gaps formed by the DNA/RNA primase PrimPol. Using BPDE and other bulky model lesions, we report that RAD51 is not recruited to stalled or collapsed forks, but instead to long gaps formed by PrimPol re-priming activity and resection by MRE11 and EXO1. In contrast, RAD51 loading at DSBs does not require PrimPol. At bulky adducts, PrimPol is required for the induction of sister chromatid exchanges and genetic recombination. Our data support that HR at bulky adducts in mammalian cells involves post-replicative gap repair and define a role for PrimPol in DNA damage tolerance by homologous recombination.

Introduction

A proper cell response to DNA damage during DNA replication is essential to maintain genome integrity and prevent cancer development. Environmental exposures frequently induce bulky DNA adducts, mutagenic and carcinogenic DNA lesions that can pose strong physical obstacles to DNA replication forks. If not removed by nucleotide excision repair (NER), then the presence of these adducts on the DNA template inhibits the replicative polymerase, potentially leading to replication fork stalling. If stalled forks cannot be restarted, they can collapse into DNA double strand breaks (DSBs), which are highly toxic and/or mutagenic. Fork collapse also activates homologous recombination (HR) for repair[1, 2].

HR proteins, such as RAD51, are also involved in the remodelling and restart of stalled forks. We previously showed that replication inhibitors such as hydroxyurea induce at least two different RAD51-mediated HR pathways.

Stalled forks recruit small amounts of RAD51 for restart, while HR repair of forks that have been collapsed into DSBs requires more extensive RAD51 loading and formation of RAD51 foci[3]. RAD51 functions at stalled forks have since then been linked to replication fork reversal[4], fork protection by preventing MRE11 resection[5], and promoting continuous replication through interaction with DNA Pol alpha[6]. Sources of bulky adducts, such as UV radiation or the environmental mutagen benzo[*a*]pyrene-diol-epoxide (BPDE), strongly induce RAD51 foci formation and HR, suggesting that these lesions stall and collapse forks[7-9]. However, bulky DNA lesions can also be bypassed using DNA damage tolerance pathways, which avoid fork stalling. Damage tolerance can occur through re-priming, for example by PrimPol, a recently described RNA/DNA primase that exerts both DNA/RNA primase and DNA polymerase activity[10] and can re-prime after UV lesions[11-14]. Damage tolerance can also occur through error-prone translesion synthesis (TLS) that is promoted by PCNA mono-ubiquitination, or an error free damage tolerance pathway that is promoted by PCNA polyubiquitination and also uses recombination proteins.

This last pathway requires RAD51 and involves template switching to the undamaged sister chromatid. Mechanistically, template switching is still poorly understood. It has been proposed to operate either directly at the stalled fork, using fork reversal, or at post-replicative gaps behind the fork, while the fork itself continues by *de novo* re-priming[15]. In budding yeast, there is evidence that re-priming and post-replicative gap filling is preferred over fork reversal, and this pathway has been shown to involve a double Holliday junction-like intermediate[16, 17]. Although it has been proposed since the 1970s that re-priming at DNA lesions can also lead to recombination in mammalian cells, fork reversal has been reported to be frequent in mammalian backgrounds[4], and may be preferred over re-priming.

Therefore, a longstanding and important mechanistic question is: where is RAD51 most important for replication bypass of bulky lesions, at the fork or behind the fork? Does the observed HR activity at bulky lesions occur at stalled forks, collapsed forks or post-replicative gaps, and what are the molecular mechanisms involved?

To address these questions, we used BPDE lesions as models to investigate HR induction at bulky DNA adducts in human cells. Like UV lesions, BPDE adducts are highly relevant to human disease. They are induced by the common environmental carcinogen benzo[a]pyrene (B[a]P). B[a]P is one of the most potent known carcinogens and ubiquitous in barbequed meat as well as emissions from traffic, industry, stoves and cigarette smoke[18, 19]. BPDE adducts cause the specific mutation signature of smoking-induced lung cancer[20, 21]. They are weak substrates for NER, and unrepaired adducts are ubiquitously detectable in the DNA of individuals[22, 23]. BPDE adducts can be bypassed in both error-free and error-prone manner by TLS polymerases[24, 25]. However, and in contrast to UV-induced cyclobutane pyrimidine dimers (CPDs), when replication encounters lower and more physiologically relevant levels of BPDE adducts, this predominantly induces HR[7, 8]. BPDE adducts are thus highly recombinogenic and excellent model lesions for studying HR at bulky adducts (Fig. 1A).

Using low concentrations of BPDE that are non-toxic and recombinogenic, we report that RAD51 foci formation and HR activation in response to bulky DNA adducts can occur in absence of replication fork stalling or -collapse. In these cases, RAD51 is recruited onto post-replicative single-stranded gaps that are generated by the re-priming activity of PrimPol, combined with resection. Our data support that HR activity at bulky adducts in mammalian cells can be associated with post-replicative repair, and define a role for PrimPol in DNA damage tolerance.

Results

RAD51 foci form at bulky DNA adducts in absence of fork stalling or -collapse

To investigate HR at bulky DNA adducts, U2OS cells were treated with BPDE for 20 min followed by release into fresh medium. After this treatment, BPDE lesions persist for more than 24 hours due to slow repair[26]. We chose a range of concentrations from low non-cytotoxic (50 nM) to high and cytotoxic doses (500 nM and 1.65 μM) (Figure S1A). BPDE induced phospho-S139 histone

H2AX (γH2AX) foci that co-localised with 5-Chlorodeoxyuridine (CldU) foci marking ongoing replication forks, supporting that the treatment was causing replication stress (Fig. 1B).

We then proceeded to quantify foci induction by BPDE. In all experiments, foci were quantified directly at the microscope, and images shown in the figures are for illustration. γH2AX foci were induced equally across all BPDE concentrations and persisted for at least 24 hours, in line with inefficient repair (Fig. 1C). RAD51 foci analysis showed that HR was induced over several days after release from BPDE. In agreement with previous studies[7, 8], the percentage of RAD51 foci positive cells was more strongly increased after release from 50 nM BPDE compared to higher BPDE doses (Fig. 1D, E). This was not due to cell cycle arrest as 50 nM BPDE had minimal effects on cell cycle distribution (Fig. S4A). Furthermore, the numbers of RAD51 foci per positive cell were also strongly increased after 50 nM BPDE (Fig S1B).

We next determined the impact of BPDE treatment on replication fork slowing and -stalling. This first required developing optimised CldU and IdU dual pulse-labelling protocols for DNA fibre analysis. We initially added BPDE with the second (IdU) label to measure the immediate effect of BPDE on replication fork progression. Only very high BPDE concentrations (1.65 μM) strongly slowed replication speeds (Fig. S1C). To measure replication fork stalling, we labelled U2OS cells with CldU before, during and for 30 min after the BPDE incubation to detect forks that stalled either during or after the treatment. Cells were then washed and labelled with IdU to detect any ongoing forks for a further 20 min (Fig. 1F). This revealed that while higher BPDE concentrations increased fork stalling, 50 nM BPDE did not lead to appreciable increase in stalled forks (Fig. 1F). This suggested that replication forks could continue progression on the damaged template under these conditions. Similar results were also obtained using fork asymmetry as a readout for fork stalling (Fig. S1D).

We previously reported that RAD51 recruitment to stalled forks does not lead to RAD51 foci formation, which instead requires fork collapse into DSBs[3]. This raised the question whether treatment with 50 nM BPDE could cause DSB formation. Analysis of 53BP1 foci, a DSB marker, and physical detection of

DSBs using pulse-field gel electrophoresis (PFGE) suggested that 50 nM BPDE induced few DSBs (Fig. 1G, Fig. S1E, F). Interestingly, highly cytotoxic treatment with 1.65 µM BPDE may suppress the DNA damage response, as the DSBs detected by PFGE did not coincide with RAD51 or 53BP1 foci induction under these conditions (Fig. 1E, G, Fig. S1F). Taken together, these data suggested that RAD51 foci induced by 50 nM BPDE were not connected with DSB formation. In contrast, RAD51 foci induced by higher BPDE concentrations correlated well with DSB formation (Fig. 1E, G). This posed the question as to the mechanism and role of RAD51 foci formation specifically after low dose BPDE treatment.

Surprisingly, siRNA depletion of RAD51 did not have a large impact on levels of stalled forks after release from low (50 nM) or high (1.65 µM) BPDE concentrations (Fig. 1H, I, Fig. S2A). This suggested that RAD51 was not required to promote fork restart under these conditions. RAD51 can also promote fork slowing or -stalling at lesions induced by UV or MMS[27, 28]. However, we found no evidence that RAD51 promoted fork slowing on BPDE-damaged templates (Fig. S2B). Furthermore, RAD51 is required for the repair of collapsed forks and prevents DSB accumulation in response to hydroxyurea[3]. However, RAD51 depletion had no major effect on the levels of 53BP1 foci induced by either 50 nM or 500 nM BPDE (Fig. 1J, Fig. S2C). These data suggested that RAD51 is also not involved in preventing fork collapse, or in repairing collapsed forks in response to BPDE lesions.

PrimPol-mediated re-priming promotes ssDNA gap formation at bulky DNA adducts

RAD51 loading to initiate HR requires formation of long stretches of ssDNA that are initially coated with RPA, which is then exchanged for RAD51. RPA foci analysis showed that ssDNA was rapidly formed even after release from 50 nM BPDE, in absence of fork stalling or DSB formation (Fig. S3A, B). RAD51 depletion impaired the resolution of these RPA foci after release from BPDE, suggesting that RAD51 was involved in resolution of BPDE-induced ssDNA (Fig. 2A).

To specifically test whether ssDNA gaps were formed at BPDE lesions behind ongoing forks, we used the S1 endonuclease (S1)-modified fibre assay[29]. S1-dependent DNA cleavage of ssDNA gaps or nicks allows to specifically detect these lesions in newly replicated DNA (Fig. 2B). After DNA fibre labelling, nuclei are permeabilised and treated with recombinant S1 nuclease before DNA fibre spreading and staining. The IdU pulse is extended to 50 min in order to capture more events, even though this leads to CldU/IdU ratios that are skewed upwards (Fig. 2C). However, if ssDNA gaps are present in nascent DNA, the S1-induced DSBs cause further shortening of the IdU-labelled fibres, thus increasing CldU/IdU ratios compared to mock-treated samples. Release from 50 nM BPDE, but not from solvent, resulted in increased CldU/IdU ratios in S1 treated- compared to mock-treated samples, supporting that ssDNA gaps were generated behind the fork during replication of DNA containing BPDE lesions (Fig. 2C). Taken together, these data suggested that RAD51 is involved in post-replicative repair and that the RAD51 foci nucleation site might be at regions of ssDNA away from the ongoing fork. We hypothesised this ssDNA might form at post-replicative gaps through re-priming of DNA synthesis downstream of the bulky lesion (Fig. 2D).

We therefore investigated a potential role for re-priming in ssDNA gap formation. The RNA/DNA primase PrimPol was recently reported to re-prime after UV lesions[11-14] and was therefore an obvious candidate for promoting ssDNA gap formation (Fig. 2D). We used siRNA[12] to deplete PrimPol in U2OS cells (Fig. 2E, S3C). We first tested whether PrimPol re-priming was responsible for the continued fork progression and lack of fork stalling after treatment with 50 nM BPDE. Indeed, we observed that 50 nM BPDE induced fork stalling specifically when PrimPol was depleted (Fig. 2F). Furthermore, PrimPol depletion prevented ssDNA gap induction behind the fork as measured by S1 nuclease fibre assay (Fig. 2G, Fig. S3D). PrimPol exerts both DNA/RNA primase and DNA polymerase activity[10]. To test whether the PrimPol primase activity is specifically required for continued replication fork progression in presence of BPDE, we performed rescue experiments by ectopically expressing wild type (WT) and primase-dead (CH) mutant versions of PrimPol[11, 30]. These experiments were performed using a U2OS cell line

carrying an inducible shRNA that would not target the ectopic constructs [7] (Fig. 2H, I), as well as siRNA depletion combined with re-expression of siRNA-resistant WT or CH mutant PrimPol variants (Fig. S3E-G). Only WT PrimPol, but not CH PrimPol, could rescue BPDE-induced fork stalling, supporting that re-priming prevents BPDE-induced fork stalling (Fig. 2J, Fig. S3G).

PrimPol-mediated re-priming and further end processing promote RAD51 loading

We next investigated whether RAD51 foci formation itself depended on PrimPol-mediated re-priming and ssDNA gap formation. PrimPol depletion in U2OS cells specifically suppressed BPDE-induced RAD51 foci formation, but did not suppress spontaneous RAD51 foci (Fig. 3A, B). BrdU incorporation confirmed that this was not due to cell cycle changes or inhibition of DNA replication after PrimPol depletion (Fig. 3C, Fig. S4A). Ongoing PrimPol depletion over the time course was confirmed using qRT-PCR (Fig. S3B). Additionally, impaired RAD51 foci formation was also observed in PrimPol-depleted epithelial lung carcinoma A549 and normal lung fibroblast MRC5 cells, and in PrimPol knock-out MRC5 cells (Fig. S4C-E).

We next performed rescue experiments to test whether PrimPol primase activity is needed for RAD51 foci formation in presence of BPDE. RAD51 foci formation in PrimPol-depleted cells could be rescued by ectopic expression of PrimPol WT, but not the primase-dead PrimPol CH mutant, again suggesting that specifically the re-priming activity is required for RAD51 foci formation (Fig. 3D). Similar results were obtained using siRNA depletion combined with expression of siRNA-resistant PrimPol variants (Fig. S4F).

In vitro experiments suggest that PrimPol re-primes around 14 nucleotides downstream of DNA lesions[31]. Such short ssDNA gaps would need further resection by nucleases such as MRE11 and Exonuclease 1 (EXO1) to allow for RAD51 foci formation (Fig. 4A). To investigate the resection of these gaps, we used Single Molecule Analysis of Resection Tracks (SMART)[32]. Cells were treated with BrdU for 48 hours to BrdU-label all DNA (Fig. 4B). DNA fibre

spreading followed by BrdU immunostaining without acid denaturation was then used to visualise stretches of ssDNA (Fig. 4C). BPDE treatment clearly induced ssDNA tracks, which required both PrimPol and EXO1 (Fig. 4C, D). In contrast, ssDNA tracks at DSBs induced by etoposide were considerably longer than BPDE-induced tracks and required EXO1, but not PrimPol (Fig. S5A). This supports that BPDE-induced ssDNA tracks were not due to resected DSBs. To further investigate the contribution of resection activities to BPDE-induced ssDNA track formation, we used PFM01, a chemical inhibitor of the endonuclease activity of MRE11 (Fig. 4E). PFM01 treatment also reduced the lengths of the ssDNA tracks (Fig. 4E, F), suggesting that initial short gaps are further extended by resection through MRE11 and EXO1.

We then investigated the impact of resection on RAD51 foci formation, using chemical inhibitors of the exo- and endonuclease activities of MRE11 (mirin and PFM01, respectively) as well as siRNA depletion of EXO1. MRE11 activity and EXO1 were both required for BPDE-induced RAD51 foci formation, supporting that PrimPol-mediated HR initiation involves resection (Fig 4G, H).

PrimPol re-priming promotes RAD51 loading at bulky DNA adducts, but not in response to DSBs

To investigate the relevance of PrimPol re-priming for HR initiation at other bulky lesions, we used UV-C irradiation to induce CPD and 6-4 photoproducts and measured the impact on ssDNA gap formation in presence and absence of PrimPol (Fig 5A). UV-C irradiation induced large amounts of S1 endonuclease-sensitive sites. While PrimPol depletion induced some S1-sensitive sites in both mock- and UV-C-irradiated samples, the UV-specific induction of S1-sensitive sites was reduced after PrimPol depletion (Fig. 5B). Furthermore, PrimPol was required for efficient RAD51 foci formation in response to bulky lesions induced by UV-C, and at bulky DNA adducts induced by the chemical carcinogen 4-nitroquinolie 1-oxide (4-NQO), which induces bulky adducts on purines (Fig. 5C, D). PrimPol requirement for RAD51 formation after UV-C was overall smaller than for BPDE and 4-NQO.

This may be partly due to recombination also being initiated by NER activity at UV lesions[33]. Taken together, these data suggest that PrimPol-mediated re-priming generates ssDNA gaps for RAD51 loading at bulky DNA adducts more widely.

We then investigated whether PrimPol is required for RAD51 foci formation under conditions where HR is initiated at DSBs. We used treatments with 2 mM HU for 24 hours, or 2 Gy of ionising radiation (IR), which both induce DSBs either via fork collapse or directly[3]. PrimPol was not required for RAD51 loading in response to DSB-inducing treatments (Fig. 5E, F). Similarly, treatment with 500 nM BPDE induces predominantly DSB-associated HR after fork stalling (Fig. 1E-G), and PrimPol was not required for RAD51 loading in response to 500 nM BPDE (Fig. S6A). PrimPol re-priming still occurred at 500 nM BPDE (Fig. S6B, C), indicating that PrimPol-mediated ssDNA gaps can be channelled into other gap filling pathways such as TLS. This observation is consistent with reports that high BPDE damage loads favour TLS over HR[7, 8]. The lack of a role for PrimPol in DSB-induced recombination agrees with the standard model of RAD51 loading onto resected DSB ends, which does not require any re-priming.

PrimPol-mediated ssDNA gap formation promotes homologous recombination and sister chromatid exchange

Finally, we investigated whether PrimPol-mediated re-priming is required to support activation of the complete HR pathway leading to genetic recombination. We analysed BPDE-induced HR frequencies using the reporter cell line SW480SN.3, which harbours the SCneo recombination reporter construct that can detect HR by unequal sister chromatid exchange, intrachromatid exchange, single-strand annealing or gene conversion[34]. 50 nM BPDE induced measurable HR in this reporter, and this was reduced after PrimPol depletion (Fig 6A, Fig. S7A). In contrast, PrimPol depletion had no effect on colony survival or percentage of sub-G1 population after BPDE treatment, and the impact of RAD51 depletion on survival was also very small

(Fig 6B, Fig. S7B). PrimPol depletion did also not increase DSB formation after BPDE treatment (Fig. S7C). This is in line with previous findings that PrimPol-depleted human cells are not very sensitive to DNA damage induced by UV, suggesting that other pathways such as TLS or fork regression can compensate[12, 35]. It also suggests that the PrimPol-mediated pathway might predominantly impact on BPDE-induced mutagenesis and/or the level of genomic rearrangements, rather than cytotoxicity. We further investigated induction of sister chromatid exchanges (SCEs) as read-out for crossover resolution of HR events. 50 nM BPDE and 50 nM 4-NQO both clearly induced SCE formation (Fig 6C-E). SCE formation is usually attributed to collapsed fork repair, but according to some models, SCEs could also arise from post-replicative template switching[36]. In support of this, PrimPol depletion prevented BPDE- and 4-NQO-induced SCE formation, while it did not influence the spontaneous induction of SCEs observed under undamaged conditions (Fig. 6D, E).

Discussion

We have shown that during DNA replication of bulky DNA adducts in mammalian cells, HR activation can occur in absence of stalled or collapsed replication forks at single-stranded gaps that are generated by the re-priming activity of PrimPol (Fig. 6F). This pathway has both similarities and differences to DSB repair.

Previous work has suggested roles for re-priming and PrimPol at UV and cisplatin lesions[9, 11-14, 37]. It is therefore to be expected that re-priming also occurs at other bulky lesions. However, our findings address long-standing questions by showing that at bulky DNA adducts, RAD51 foci formation and sister chromatid exchange that have been traditionally connected with replication fork collapse and DSB repair, are associated with the repair of post-replicative gaps. Furthermore, these post-replicative gaps are produced by PrimPol, shedding light on the function of PrimPol during DNA damage tolerance.

Most DNA damaging or replication blocking treatments cause fork slowing and/or stalling as well as fork reversal[4]. The previously described functions of RAD51 at such forks are therefore likely to be active during most forms of replication stress. However, we suggest that in addition to fork reversal, fork restart and the repair of collapsed forks, HR at post-replicative gaps constitutes an additional important function of RAD51 in response to replication blocks. There could be competition between several of these pathways. It was recently reported that PrimPol repriming competes with replication fork reversal in response to cisplatin lesions[37].

Why are these post-replicative gaps resected and channelled into HR rather than simply filled by TLS? We speculate that HR and TLS-dependent gap filling could compete at ssDNA gaps. Gap resection might prevent TLS and promote HR, but TLS might be preferred over resection under high damage load. It will be important to decipher whether and how PrimPol re-priming and the presence of the bulky adduct influence the pathway decision between TLS and template switching.

Our data agree with recent work in budding yeast, reporting that checkpoint activation by fork-stalling lesions also occurs at EXO1-resected post-replicative gaps rather than directly at the fork[38]. Furthermore, EXO1 resection is downstream of PCNA polyubiquitylation that promotes template switching. A model was proposed in which resection of the gap is stimulated by polyubiquitylated PCNA stuck on the 3’ (upstream) junction and by the 9-1-1 checkpoint clamp loaded onto the 5’ (downstream) junction[39] (Fig. 6F). The length of BPDE-induced gaps will require further investigation to determine whether PrimPol can re-prime far away from the lesion, and/or whether long-range resection takes place.

With the observed roles for resection and RAD51 foci formation, HR at bulky adducts seems to resemble DSB repair more than the known HR functions at stalled forks. It has been speculated pro-recombination activities could be specifically recruited to the post-replicative environment at the gap[15]. These may promote RAD51 foci formation, and long-range resection may support more accurate homology search. In contrast at stalled replication forks,

RAD51 foci formation might be suppressed by anti-recombinogenic helicase activities[15] and the possibilities for remodelling, e.g. by fork reversal (Fig. 6F).

Another unanswered question is the contribution of re-priming by DNA polymerase α (Pol α) to HR. Pol α is solely responsible for gap formation in yeast, which lack PrimPol[17]. In mammalian cells, with Pol α constantly re-priming on the lagging strand and possibly also the leading strand, one would expect at most half of gap- and RAD51 foci formation to be PrimPol-dependent. Recent work has suggested that in budding yeast, different pathways act on the leading and lagging strands[40] it will be interesting to investigate whether only re-priming via PrimPol promotes HR-dependent gap repair, possibly due to PrimPol's preference to synthesise DNA primers.

While we have shown that PrimPol re-priming initiates HR at UV, 4-NQO and BPDE DNA adducts, it will be interesting to investigate whether other bulky lesions or replication impediments can be channelled into this pathway. DNA-protein crosslinks for example engage HR for repair[41, 42] and lead to template-switching[43] raising the question whether PrimPol could act at these lesions as well. PrimPol also re-primes at R-loops and secondary structure-forming sequences[44, 45] , opening up the possibility that HR in those backgrounds might depend at least partially on PrimPol. It will be important to test how commonly PrimPol promotes recombination at other replication-blocking structures.

Understanding the molecular mechanism of HR induced by bulky adducts is important for human health. We suggest that this will be particularly useful to interpret more recent cancer genomics data. Both BPDE-treated cells and lung cancers harbour insertion and deletion mutations (indels) of unknown origin. These are in addition to the point mutations ascribed to error-prone TLS[20, 46]. Indels could result from replication-associated HR, such as at restarting forks [47], or from defective HR, such as in BRCA-mutant cancers[48]. It is therefore important to decipher which HR pathways are actually induced by bulky adducts. Furthermore, genetic variants in the HR genes *BRCA2* and *RAD52* have been liked to lung cancer susceptibility[49, 50]. It will be important to investigate the impact of such genetic variants on HR at ssDNA gaps. A *PRIMPOL* variant has also been suggested to play a potential role in cancer[51].

Taken together, our data support that a large fraction of mammalian replication-associated HR can occur after re-priming, post-replicatively behind the fork.

Materials and Methods

Cell lines and reagents

U2OS, A549 and MRC5 cells were obtained from ATCC. The SW480SN.3[52], PrimPol$^{-/-}$ MRC5[35], and U2OS cell lines carrying doxycycline (Dox)-inducible PrimPol shRNA[11] have been described before. Cells were confirmed to be free of Mycoplasma infection and grown in Dulbecco's modified Eagle's Medium (DMEM) with 10% foetal bovine serum in a humidified atmosphere containing 5% CO_2. MRC WT and PrimPol$^{-/-}$ cells were grown in Minimum Essential Media (MEM) with 15% foetal bovine serum. Media was additionally supplemented with L-Glutamine (2 mM), Penicillin (50 U/mL), and Streptomycin (50 µg/mL) for all cell lines. Additionally, SW480SN.3 cells were grown in hygromycin (50 µM) to maintain the SCneo recombination reporter.

(+)-*anti*-B[a]P-7*R*,8S-dihydrodiol-9*S*,10*R*-epoxide (enantiopure, BPDE) was custom-synthesised by the Biochemical Institute for Environmental Carcinogens (Grosshansdorf, Germany). Mirin, PFM01, 4-nitroquinolie 1-oxide (4-NQO), etoposide and hydroxyurea (HU) were from Sigma-Aldrich.

Immunofluorescence

Cells were fixed with 4% PFA for 10 min and permeabilised with 0.25% triton X-100 for 5 min at 4°C followed by blocking with 4% FCS in PBS. Primary antibodies were rabbit polyclonal anti-RAD51 (Abcam ab63801, 1:800 or Calbiochem PC130, 1:2,000 for IR-induced RAD51 foci), mouse monoclonal anti-phospho-Histone H2AX (Ser139) (JBW301, Millipore, 1:1,000), rabbit polyclonal anti-53BP1 (Bethyl A300-272A, 1:15,000), mouse anti-RPA32 (Merck NA18, 1:500), rat anti-BrdU (BU1/75, Abcam ab6326, 1:250) to detect CldU. Secondary antibodies were anti-rabbit IgG AlexaFluor 555 and anti-mouse IgG AlexaFluor 488 (ThermoFisher). For RPA staining, cells were pre-extracted with CSK buffers (CSK1: 10 mM PIPES, 300 mM sucrose, 100 mM NaCl, 3 mM $MgCl_2$, CSK2: 0.5 % Triton X-100) on ice previous to PFA

fixation. For RAD51 foci detection in response to IR irradiation, cells were also pre-extracted and subjected to EdU staining to label replicating cells. To this end, cells were incubated with EdU at a final concentration of 1 μM for 30 min before staining was carried out as detailed in Click-iT EdU Imaging Kits (Life Technologies). For co-localisation staining, primary and secondary antibodies against phospho-Histone H2AX were fixed for 10 min with 2% PFA before DNA denaturation with 2M HCl for 40 min and immunostaining for CldU. DNA was counterstained with DAPI. Cells with more than 5 RAD51 foci (10 foci for IR-induced RAD51 staining) and 8 γH2AX or 10 53BP1 foci were scored as positive. Foci were quantified directly on the microscope, and representative images were taken for illustration.

DNA fibre analysis

U2OS cells were pulse labelled with 25 μM CldU and 250 μM IdU, and treated with BPDE for the times indicated. Labelled cells were harvested and DNA fibre spreads were incubated with rat anti-BrdU (BU1/75, Abcam ab6326, 1:700) and mouse anti-BrdU (B44, Becton Dickinson 347580, 1:500) for 1 h, fixed with 4% PFA and incubated with anti-rat AlexaFluor 594 and anti-mouse AlexaFluor 488 (Thermo Fisher) for 1.5 h. Fibers were examined using a Nikon E600 microscope with a Nikon Plan Apo 60x (1.3 NA) oil lens, a Hamamatsu digital camera (C4742-95) and the Volocity acquisition software (Perkin Elmer). For quantification of replication structures, at least 190 structures were counted per experiment. For quantification of fork speeds, the lengths of labelled tracks were measured using the ImageJ software (http://rsbweb.nih.gov/ij/)[53] and arbitrary length values were converted into μm using a micrometer slide for calibration. Fork stalling was quantified either by scoring percentages of CldU-only fibres of all red-labelled structures or by comparing the lengths of IdU tracks of bidirectional forks (fork asymmetry).

S1 endonuclease (S1)-modified DNA fibre assay

The S1-modified DNA fibre assay was carried out as described before[29]. Briefly, U2OS cells were pulse labelled with 25 μM CldU and 250 μM IdU, and treated with BPDE for the times indicated followed by permeabilization with CSK100 buffer (100 mM NaCl, 10 mM MOPS pH 7.0, 3 mM $MgCl_2$, 300 mM

sucrose, 0.5% triton X-100) for 10 min. Nuclei were subsequently treated with either 20 U/mL S1 endonuclease (Invitrogen, 18001016) to induce DSBs at sites of DNA gaps or mock-treated (S1 buffer: 30 mM sodium acetate, 10 mM zinc acetate, 5% glycerol, 50 mM NaCl, pH 4.6) for 30 min at 37°C. Nuclei were harvested by scraping and DNA fibre spreads were prepared, stained and analysed as described for the unmodified fibres assay above. At least 120 fibres per condition were measures from 3 independent biological repeats.

Single Molecule Analysis of Resection Tracks (SMART)

SMART assay was performed as described[54]. U2OS cells were treated with 20 µM BrdU for 48 h. After treatment with BPDE, siRNA, etoposide or MRE11 inhibitor as applicable, DNA was spread as for the unmodified DNA fibre assay. Native fibre spreads were stained with mouse anti-BrdU (B44, Becton Dickinson 347580, 1:500) for 1 h, fixed with 4% PFA and incubated with anti-mouse AlexaFluor 488 (Thermo Fisher) for 1.5 h. Fibers were examined as described above. For quantification of DNA gap sizes, the lengths of green (AF 488) labelled native patches were measured using ImageJ and arbitrary length values were converted into µm using the scale bars created by the microscope. A total of at least 550 fibre stretches derived from 3 independent biological repeats were measured.

Pulsed-field gel electrophoresis (PFGE)

To detect DSBs, $2x10^6$ cells per sample were treated as indicated, harvested and melted into 1.0% InCert-Agarose (Lonza) inserts. Inserts were digested in 0.5 M EDTA-1% *N*-laurylsarcosyl-proteinase K (1 mg/ml) at room temperature for 48 h and washed three times in TE buffer. Inserts were loaded onto a separation gel (1.0% chromosomal-grade agarose, Bio-Rad). Separation was performed using a CHEF DR III (BioRad; 120 field angle, 240 s switch time, 4 V cm^{-1}, 14 °C) for 20 h. Images of ethidium bromide-stained gels were acquired using a Syngene G:BOX gel imaging system. DSBs (chromosome fragments >2 Mbp) were quantified by densitometry using ImageJ and normalized to the total amount of DNA in the gel.

siRNA and DNA transfection

Custom made siRNAs against RAD51[55] , and PrimPol[12] were from Dharmacon, and custom made EXO1 siRNA (Sense: GAA CAA GGU UCC UGG GCU AUA[dT][dT], Antisense: [Phos]UAU AGC CCA GGA ACC UUG UUC[dT][dT]) was from Sigma-Aldrich. “Allstars negative control siRNA” was from Qiagen. Cells were transfected for 48 h with 50 nM siRNA using Dharmafect 1 reagent (Dharmacon). Expression of PrimPol shRNA was induced with 1 µg/ml Dox for 3 d. For rescue experiments, 2.5 µg of PrimPol variant expressing pcDNA3.1/nV5-DEST vectors[11] or control plasmid pEGFP-C2 (Clontech) were transfected for the last 24 h using TransIT-2020 (Mirus Bio). To generate siRNA-resistant expression vectors, pcDNA3.1/nV5-DEST vectors expressing PrimPol WT or CH variant[11] were subjected to site-directed mutagenesis using forward primer CGT CTG TGT ACA GAC CAA GAT TGT CCA AG; reverse primer ACA AGG GCT TTC TCT CAT AAT GAG ATG CTC and the Q5® Site-Directed Mutagenesis Kit (New England Biolabs). Cells were transfected with 50 nM siRNA using Dharmafect 1 for 48 h, and with 2.5 µg siRNA-resistant expression vectors or pEGFP-C2 using TransIT-2020 for the last 24 h.

Western blotting

Cell extracts were prepared in UTB buffer (50 mM Tris-HCl pH 7.5, 150 mM β-mercaptoethanol, 8 M urea) and sonicated to release DNA-bound proteins. Primary antibodies used were rabbit anti-RAD51 (Abcam, ab63801, 1:1,000), rabbit anti-EXO1 (Bethyl, A302-640, 1:1,000), rabbit anti-PRIMPOL (described in ref[11]), rabbit anti-SMC1 (a kind gift from A. Losada’s lab, CNIO[56]), mouse anti-V5 tag (Invitrogen, R960-25, 1:1:500), and mouse anti-αTUBULIN (B512, Sigma T6074, 1:10,000).

Quantitative RT-PCR

Total RNA was harvested using the miRNeasy Mini Kit (Qiagen) followed by DNase I treatment (Roche). 1 µg of total RNA was reverse-transcribed using SuperScript Reverse Transcriptase III (Thermo Fisher) with random primers (Promega), following manufacturer’s instructions. The qPCR primers for amplification are listed in Table S1. For quantitative RT-PCR, 2 µl of cDNA

were analyzed using a CFX Connect real-time PCR machine (BioRad) with SensiFAST SYBR Lo-ROX Kit (Bioline). Cycling parameters were 95°C for 3 min, followed by 40 cycles of 95°C for 10 s, 60°C for 30 s. Result were normalised to RPLP0. ∆cT was calculated as difference in the cycle threshold of the transcript of interest and RPLP0, plotted as fold change compared to the CTR untreated sample.

Recombination in SW480SN.3 cells

Following siRNA treatments, SW480SN.3 cells were rinsed in PBS and left in fresh non-selective media for 48 h. Cells were treated with solvent or 50 nM BPDE for 20 min, rinsed in 2x PBS, trypsinized and directly reseeded. To determine cloning efficiency, two dishes were plated with 500 cells each. For selection of recombinants cells were grown in G418 (1 mg/ml; 25 cells/mm^2) in two technical repeats. After 14-18 days the colonies obtained were stained with methylene blue in methanol (4 g/l) and the number of recombinants was calculated per 10^{-5} colony forming cells. Recombination frequencies were normalised to BPDE-treated samples to account for the high variation in spontaneous recombination between samples.

Analysis of sister chromatid exchange (SCE)

U2OS were incubated with 240 µM BrdU for two cell cycles and treated with BPDE, 4-NQO, or siRNA as indicated, and SCE analysis was performed as described[57]. SCEs were defined by an exchange of dark-stained (Hoechst-bound TT-rich) segments with light, bleached (BrdU incorporated) segments. Staining variation where chromatids clearly twisted around each other was excluded from the count. For each condition, at least 90 metaphases from at least 3 independent biological repeats were analysed. SCE rates were calculated per diploid set of chromosomes to compensate although U2OS present with chromosome counts in the hypertriploid range. SCEs were quantified directly on the microscope, and representative images were taken for illustration.

Colony survival assay

U2OS cells were siRNA transfected for 24 h previous to being plated in triplicates for both 500 and 1,000 cells. Cells were given 24 h to adhere before

treatment with BPDE (10 – 400 nM) for 20 min. Subsequently, cells were washed 2 x PBS and colonies of >50 cells were allowed to form in fresh medium and fixed in 50% ethanol, 2% methylene blue.

Flow cytometry

U2OS cells were transfected with siRNA for 48 h followed by treatment with 50 nM BPDE and release into fresh DMEM. Cells were incubated with 100 µM BrdU for the last 30 min of the indicated release times and then fixed in 70% ethanol overnight. Cells were incubated in 2 M HCl/0.1mg/ml pepsin for 30 min. Samples were washed in PBS before incubation with mouse anti-BrdU (B44, Becton Dickinson 347580, 1:200) for 1 h and subsequently with anti-mouse IgG AlexaFluor 488 (ThermoFisher) for 1 h. Finally, cells were incubated with 10 µg/ml propidium iodide and 25 µg/ml RNaseA for 30 min. Cell cycle profiles were gathered using the BD LSR Fortessa X20 and analysed with BD FacsDiva software.

Quantification and statistical analysis

Values represent the means + 1x SEM of at least 3 independent biological repeats. For foci analysis, at least 10 different areas with at least 140 cells in total were quantified for each independent biological repeat. The number of independent biological repeats (n) is indicated in the figure legends. The statistical tests used throughout were the one-tailed student's t-test, one-way ANOVA followed by Dunnett or Sidak test, or Mann-Whitney as indicated in the figure legends. Asterisks compare to control, unless indicated otherwise in the figure panels, and signify *$p<0.05$, **$p<0.01$, ***$p<0.001$.

References

1. Arnaudeau, C., Lundin, C. & Helleday, T. DNA double-strand breaks associated with replication forks are predominantly repaired by homologous recombination involving an exchange mechanism in mammalian cells. *J Mol Biol* **307**, 1235-1245 (2001).

2. Saintigny, Y. *et al.* Characterization of homologous recombination induced by replication inhibition in mammalian cells. *Embo J* **20**, 3861-3870 (2001).

3. Petermann, E., Orta, M.L., Issaeva, N., Schultz, N. & Helleday, T. Hydroxyurea-stalled replication forks become progressively inactivated and require two different RAD51-mediated pathways for restart and repair. *Mol Cell* **37**, 492-502 (2010).

4. Zellweger, R. *et al.* Rad51-mediated replication fork reversal is a global response to genotoxic treatments in human cells. *J Cell Biol* **208**, 563-579 (2015).

5. Schlacher, K. *et al.* Double-Strand Break Repair-Independent Role for BRCA2 in Blocking Stalled Replication Fork Degradation by MRE11. *Cell* **145**, 529-542 (2011).

6. Kolinjivadi, A.M. *et al.* Smarcal1-Mediated Fork Reversal Triggers Mre11-Dependent Degradation of Nascent DNA in the Absence of Brca2 and Stable Rad51 Nucleofilaments. *Mol Cell* **67**, 867-881.e867 (2017).

7. Izhar, L., Ziv, O., Cohen, I.S., Geacintov, N.E. & Livneh, Z. Genomic assay reveals tolerance of DNA damage by both translesion DNA synthesis and homology-dependent repair in mammalian cells. *Proc Natl Acad Sci U S A* **110**, E1462–E1469 (2013).

8. Cohen, I.S. *et al.* DNA lesion identity drives choice of damage tolerance pathway in murine cell chromosomes. *Nucleic Acids Research* **43**, 1637-1645 (2015).

9. Elvers, I., Johansson, F., Groth, P., Erixon, K. & Helleday, T. UV stalled replication forks restart by re-priming in human fibroblasts. *Nucleic Acids Res* **39**, 7049-7057 (2011).

10. Guilliam, T.A. & Doherty, A.J. PrimPol-Prime Time to Reprime. *Genes* **8** (2017).

11. Mourón, S. *et al.* Repriming of DNA synthesis at stalled replication forks by human PrimPol. *Nat Struct Mol Biol* **20**, 1383-1389 (2013).

12. Bianchi, J. *et al.* PrimPol bypasses UV photoproducts during eukaryotic chromosomal DNA replication. *Mol Cell* **52**, 566-573 (2013).

13. Garcia-Gomez, S. *et al.* PrimPol, an archaic primase/polymerase operating in human cells. *Mol Cell* **52**, 541-553 (2013).

14. Keen, B.A., Jozwiakowski, S.K., Bailey, L.J., Bianchi, J. & Doherty, A.J. Molecular dissection of the domain architecture and catalytic activities of human PrimPol. *Nucleic Acids Res* **42**, 5830-5845 (2014).

15. Branzei, D. & Szakal, B. Building up and breaking down: mechanisms controlling recombination during replication. *Critical reviews in biochemistry and molecular biology* **52**, 381-394 (2017).

16. Giannattasio, M. *et al.* Visualization of recombination-mediated damage bypass by template switching. *Nat Struct Mol Biol* **21**, 884-892 (2014).

17. Fumasoni, M., Zwicky, K., Vanoli, F., Lopes, M. & Branzei, D. Error-free DNA damage tolerance and sister chromatid proximity during DNA replication rely on the Polalpha/Primase/Ctf4 Complex. *Mol Cell* **57**, 812-823 (2015).

18. IARC A review of human carcinogens: Chemical agents and related occupations. *IARC Monographs on the Evaluation of Carcinogenic Risks to Humans* **100F**, 111-144 (2012).

19. Choi, H., Komulainen, H. & Delgado Saborit, J.M. 289-346 (WHO Regional Office for Europe, 2010).

20. Alexandrov, L.B. *et al.* Mutational signatures associated with tobacco smoking in human cancer. *Science* **354**, 618-622 (2016).

21. Kucab, J.E. *et al.* A Compendium of Mutational Signatures of Environmental Agents. *Cell* **177** (2019).

22. Geacintov, N.E. & Broyde, S. Repair-Resistant DNA Lesions. *Chem Res Toxicol* **30**, 1517-1548 (2017).

23. Villalta, P.W., Hochalter, J.B. & Hecht, S.S. Ultrasensitive High-Resolution Mass Spectrometric Analysis of a DNA Adduct of the Carcinogen Benzo[a]pyrene in Human Lung. *Analytical chemistry* **89**, 12735-12742 (2017).

24. Rechkoblit, O., Kolbanovskiy, A., Landes, H., Geacintov, N.E. & Aggarwal, A.K. Mechanism of error-free replication across benzo[a]pyrene stereoisomers by Rev1 DNA polymerase. *Nature communications* **8**, 965 (2017).

25. Livneh, Z., Ziv, O. & Shachar, S. Multiple two-polymerase mechanisms in mammalian translesion DNA synthesis. *Cell Cycle* **9**, 729-735 (2010).

26. Piberger, A.L., Kruger, C.T., Strauch, B.M., Schneider, B. & Hartwig, A. BPDE-induced genotoxicity: relationship between DNA adducts, mutagenicity in the in vitro PIG-A assay, and the transcriptional response to DNA damage in TK6 cells. *Archives of toxicology* **92**, 541-551 (2018).

27. Vallerga, M.B., Mansilla, S.F., Federico, M.B., Bertolin, A.P. & Gottifredi, V. Rad51 recombinase prevents Mre11 nuclease-dependent degradation and excessive PrimPol-mediated elongation of nascent DNA after UV irradiation. *Proc Natl Acad Sci U S A* **112**, E6624-6633 (2015).

28. Ronson, G.E. *et al.* PARP1 and PARP2 stabilise replication forks at base excision repair intermediates through Fbh1-dependent Rad51 regulation. *Nature communications* **9**, 746 (2018).

29. Quinet, A., Carvajal-Maldonado, D., Lemacon, D. & Vindigni, A. DNA Fiber Analysis: Mind the Gap! *Methods in enzymology* **591**, 55-82 (2017).

30. Martinez-Jimenez, M.I., Calvo, P.A., Garcia-Gomez, S., Guerra-Gonzalez, S. & Blanco, L. The Zn-finger domain of human PrimPol is required to stabilize the initiating nucleotide during DNA priming. *Nucleic Acids Res* (2018).

31. Kobayashi, K. *et al.* Repriming by PrimPol is critical for DNA replication restart downstream of lesions and chain-terminating nucleosides. *Cell Cycle* **15**, 1997-2008 (2016).

32. Cruz-Garcia, A., Lopez-Saavedra, A. & Huertas, P. BRCA1 accelerates CtIP-mediated DNA-end resection. *Cell Rep* **9**, 451-459 (2014).

33. Ma, W., Westmoreland, J.W. & Resnick, M.A. Homologous recombination rescues ssDNA gaps generated by nucleotide excision repair and reduced translesion DNA synthesis in yeast G2 cells. *Proc Natl Acad Sci U S A* **110**, E2895-2904 (2013).

34. Johnson, R.D., Liu, N. & Jasin, M. Mammalian XRCC2 promotes the repair of DNA double-strand breaks by homologous recombination. *Nature* **401**, 397-399 (1999).

35. Bailey, L.J., Bianchi, J. & Doherty, A.J. PrimPol is required for the maintenance of efficient nuclear and mitochondrial DNA replication in human cells. *Nucleic Acids Res* (2019).

36. Dong, Z. & Fasullo, M. Multiple recombination pathways for sister chromatid exchange in Saccharomyces cerevisiae: role of RAD1 and the RAD52 epistasis group genes. *Nucleic Acids Res* **31**, 2576-2585 (2003).

37. Quinet, A. *et al.* PRIMPOL-Mediated Adaptive Response Suppresses Replication Fork Reversal in BRCA-Deficient Cells. *Mol Cell* (2019).

38. Garcia-Rodriguez, N., Morawska, M., Wong, R.P., Daigaku, Y. & Ulrich, H.D. Spatial separation between replisome- and template-induced replication stress signaling. *EMBO J* **37** (2018).

39. Garcia-Rodriguez, N., Wong, R.P. & Ulrich, H.D. The helicase Pif1 functions in the template switching pathway of DNA damage bypass. *Nucleic Acids Res* **46**, 8347-8356 (2018).

40. Rosenbaum, J.C. *et al.* The Rad51 paralogs facilitate a novel DNA strand specific damage tolerance pathway. *Nature communications* **10**, 3515 (2019).

41. Nakano, T. *et al.* Nucleotide excision repair and homologous recombination systems commit differentially to the repair of DNA-protein crosslinks. *Mol Cell* **28**, 147-158 (2007).

42. Fang, Q. DNA-protein crosslinks processed by nucleotide excision repair and homologous recombination with base and strand preference in E. coli model system. *Mutat Res* **741-742**, 1-10 (2013).

43. Laranjo, L.T., Klaric, J.A., Pearlman, L.R. & Lovett, S.T. Stimulation of Replication Template-Switching by DNA-Protein Crosslinks. *Genes* **10** (2018).

44. Svikovic, S. *et al.* R-loop formation during S phase is restricted by PrimPol-mediated repriming. *Embo j* (2018).

45. Schiavone, D. *et al.* PrimPol Is Required for Replicative Tolerance of G Quadruplexes in Vertebrate Cells. *Mol Cell* **61**, 161-169 (2016).

46. Schiltz, M. *et al.* Characterization of the mutational profile of (+)-7R,8S-dihydroxy-9S,10R-epoxy-7,8,9,10-tetrahydrobenzo[a]pyrene at the hypoxanthine (guanine) phosphoribosyltransferase gene in repair-deficient Chinese hamster V-H1 cells. *Carcinogenesis* **20**, 2279-2286 (1999).

47. Carr, A.M. & Lambert, S. Replication stress-induced genome instability: the dark side of replication maintenance by homologous recombination. *J Mol Biol* **425**, 4733-4744 (2013).

48. Zamborszky, J. *et al.* Loss of BRCA1 or BRCA2 markedly increases the rate of base substitution mutagenesis and has distinct effects on genomic deletions. *Oncogene* **36**, 746-755 (2017).

49. Lieberman, R. *et al.* Functional characterization of RAD52 as a lung cancer susceptibility gene in the 12p13.33 locus. *Mol Carcinog* **55**, 953-963 (2016).

50. Wang, Y. *et al.* Rare variants of large effect in BRCA2 and CHEK2 affect risk of lung cancer. *Nat Genet* **46**, 736-741 (2014).

51. Diaz-Talavera, A. *et al.* A cancer-associated point mutation disables the steric gate of human PrimPol. *Sci Rep* **9**, 1121 (2019).

52. Saleh-Gohari, N. *et al.* Spontaneous homologous recombination is induced by collapsed replication forks that are caused by endogenous DNA single-strand breaks. *Molecular and Cellular Biology* **25**, 7158-7169 (2005).

53. Schneider, C.A., Rasband, W.S. & Eliceiri, K.W. NIH Image to ImageJ: 25 years of image analysis. *Nat Methods* **9**, 671-675 (2012).

54. Densham, R.M. *et al.* Human BRCA1-BARD1 ubiquitin ligase activity counteracts chromatin barriers to DNA resection. *Nat Struct Mol Biol* **23**, 647-655 (2016).

55. Ito, M. *et al.* Rad51 siRNA delivered by HVJ envelope vector enhances the anti-cancer effect of cisplatin. *J Gene Med* **7**, 1044-1052 (2005).

56. Kojic, A. *et al.* Distinct roles of cohesin-SA1 and cohesin-SA2 in 3D chromosome organization. *Nat Struct Mol Biol* **25**, 496-504 (2018).

57. Hoh, L. *et al.* Atypically low spontaneous sister chromatid exchange formation in uveal melanoma. *Genes Chromosomes Cancer* **50**, 34-42 (2011).

Acknowledgements

We thank Drs Rebecca M. Jones, Katarzyna Starowicz and Karen Sisley for advice on PFGE and SCE quantification, and Dr Ana Losada for the kind gift of anti-SMC1 antibody. This work was supported by the German Research Foundation PI 1300/1-1 (A.L.P.), Medical Research Council MR/S021310/1 (A.L.P. and E.P.), Cancer Research UK Birmingham Centre Development Fund (E.P.), Cancer Research UK 28275 (E.P.), Cancer Research UK C8820/A19062 (A.K.W. and J.R.M.), Wellcome Trust 206343/Z/17/Z (J.R.M.), University of Sheffield 322149 (H.E.B.), Biotechnology and Biological Science Research Council BB/H019723/1 and BB/M008800/1 (A.J.D.), and the Spanish Ministry of Science and Innovation BFU2016-80402-R, co-financed by E.U. ERDF funds (J.M.).
This is a preprint of an article published in *Nature Communications*. The final authenticated version is available online at: https://doi.org/10.1038/s41467-020-19570-7.

Author contributions

A.L.P. conceived the study; A.L.P., A.B., R.D.W.K., D.G., L.J.B., A.K.W., S. M-H. and H.E.B. performed the experiments; A.L.P., A.K.W., J.M., A.J.D, J.R.M., H.E.B. and E.P. designed the experiments; A.L.P. and E.P. and wrote the paper.

Declaration of Interests

The authors declare that they have no competing financial interest.

Figure Legends

Figure 1. Bulky DNA adducts induce RAD51 foci formation in absence of replication fork stalling or -collapse.

(A) Schematic of DNA repair and damage tolerance pathways induced by low doses of BPDE, which forms bulky adducts on guanine. NER: nucleotide excision repair; TLS: translesion synthesis; HR: homologous recombination.

(B) Co-localisation of γH2AX and replication forks in U2OS cells after 1 h release from 1650 nM BPDE treatment for 20 min. DNA was denatured with HCl to allow CldU detection. Cells were immunostained for CldU (red) and γH2AX (green). Scale bars are 10 µm.

(C) Percentages of U2OS cells with > 8 γH2AX foci after release from increasing concentrations of BPDE for the times indicated. n=3

(D) Representative images of BPDE-induced RAD51 foci.

(E) Percentages of U2OS cells with > 5 RAD51 foci after release from increasing concentrations of BPDE for the times indicated. n=3

(F) Percentages of stalled forks after release from BPDE. U2OS cells were pulse labelled with CldU, treated with BPDE during the CldU pulse, and released into IdU. n=4 (1650 nM n=3).

(G) Percentages of cells with > 10 53BP1 foci after release from increasing concentrations of BPDE for the times indicated. n=3

(H) Top: Protein levels of RAD51 and α-Tubulin (loading control) in U2OS cells after 48 h depletion with RAD51 or non-targeting (nonT) siRNA. Bottom: Strategy for DNA fibre labelling.

(I) Percentages of stalled forks after release from 50 nM BPDE as shown in (H) in cells treated with nonT or RAD51 siRNA for 48 h. n=3

(J) Percentages of control- or RAD51-depleted U2OS cells with > 10 53BP1 foci after release from 50 nM BPDE. n=3

The means and SEM (bars) of at least three independent experiments are shown. Asterisks indicate p-values compared to control unless indicated otherwise (one-way ANOVA and Dunnett's test for C, E, F, G; student's t-test for I, J, * $p < 0.05$, ** $p < 0.01$, *** $p < 0.001$).

Figure 2. Post-replicative single-stranded DNA gaps are generated at bulky adducts through re-priming by PrimPol.

(A) Percentages of control- or RAD51-depleted U2OS cells with > 10 RPA foci after release from BPDE for the times indicated. n=3

(B) Schematic of the S1 endonuclease-modified DNA fibre assay and strategy for DNA fibre labelling.

(C) CldU/IdU ratios after S1-modified DNA fibre assay in cells treated with solvent or 50 nM BPDE as in (B).

(D) Schematic of RAD51-mediated ssDNA gap repair after re-priming at replication-blocking lesions.

(E) Protein levels of PrimPol and SMC1 (loading control) after 6 h release from 50 nM BPDE or solvent (-) in U2OS cells after 48 h depletion with PrimPol or non-targeting (nonT) siRNA.

(F) Quantification of stalled forks after release from 50 nM BPDE in presence of non-targeting (nonT) or PrimPol siRNA. n=3

(G) CldU/IdU ratios after S1-modified DNA fibre assay in cells treated with 50 nM BPDE as in (B) after 48 h of control or PrimPol siRNA.

(H) Top: Protein domain structure of wild type (WT) and primase-dead (CH) PrimPol variants. The CH variant has two point mutations (CH > GY) in the zinc finger (ZnF) domain. Bottom: Protocol for dox-inducible shRNA depletion of endogenous PrimPol and ectopic expression of V5 tagged PrimPol variants.

(I) Protein levels of ectopic V5-tagged WT or CH PrimPol, endogenous PrimPol (long exposure, lane 1 and 4), and SMC1 (loading control) in U2OS cells after treatment as indicated above. Controls (-) were transfected with GFP expression vector.

(J) Quantification of stalled forks after release from 50 nM BPDE with or without PrimPol shRNA and expression constructs encoding GFP (-) or WT or CH PrimPol. Fibre labelling was according to (F) n=3

The means and SEM (bars) of at least three independent experiments are shown. Asterisks indicate p-values compared to control unless indicated otherwise (student's t-test for A, F, Mann-Whitney for C, G; one-way ANOVA for J, * $p < 0.05$, ** $p < 0.01$, *** $p < 0.001$).

Figure 3. PrimPol-mediated re-priming promotes RAD51 loading in response to bulky DNA adducts.

(A) Representative images of RAD51 foci after 24 h release from 50 nM BPDE in presence of nonT or PrimPol siRNA. Scale bars are 10 µm.

(B) Percentages of U2OS cells with >5 RAD51 foci after release from 50 nM BPDE for the times indicated, in presence of nonT or PrimPol siRNA. n=3

(C) Representative cell cycle distributions after release from solvent (1 h) or 50 nM BPDE in presence of nonT or PrimPol siRNA. Cells were labelled with BrdU for 30 min to label replicating cells prior to flow cytometry.

(D) Percentages of cells with >5 RAD51 foci after release from 50 nM BPDE for the times indicated, with or without PrimPol shRNA depletion and expression constructs encoding GFP or WT or CH PrimPol. n=3

The means and SEM (bars) of at least three independent experiments are shown. Asterisks indicate p-values (student's t-test for A or one-way ANOVA for D, * $p < 0.05$, ** $p < 0.01$).

Figure 4. RAD51 loading at PrimPol-dependent single-stranded DNA gaps requires DNA end resection.

(A) Schematic representation of MRE11's nuclease activities and respective chemical inhibitors PFM01 and mirin.

(B) Top: Strategy for SMART analysis of single-stranded DNA quantifications. Bottom: Protein levels of EXO1 and α-Tubulin (loading control) in U2OS cells after 48 h depletion with EXO1 or nonT siRNA.

(C) Representative images of native BrdU tracts in response to BPDE with siRNA depletion of PrimPol or EXO1. Scale bars: 10 µm.

(D) SMART analysis of single-stranded DNA after release from 20 min of 50 nM BPDE or solvent (-) for 4 h, in presence of nonT (-), PrimPol, or EXO1 siRNA.

(E) Strategy for SMART analysis with MRE11 inhibitor PFM01 and representative images of native BrdU tracts. Scale bars: 5 µm.

(F) SMART analysis of single-stranded DNA after release from 20 min of 50 nM BPDE for 4 h, in presence or absence of MRE11 inhibitor PFM01.

(G) Percentages of cells with >5 RAD51 foci after release from 50 nM BPDE for the times indicated, in presence or absence of MRE11 inhibitors mirin or PFM01. Treatment was as shown in (E). n=3
(H) Percentages of cells with >5 RAD51 foci after release from 50 nM BPDE for the times indicated, in presence of nonT or EXO1 siRNA for 48 h. n=3
The means and SEM (bars) of at least three independent experiments are shown. Asterisks indicate p-values (Mann-Whitney for D, F, one-way ANOVA for G, or student's t-test for H, * $p < 0.05$, ** $p < 0.01$, *** $p < 0.001$).

Figure 5. PrimPol promotes RAD51 foci formation specifically in response to bulky adducts.
(A) Strategy for the S1-modified DNA fibre assay with UV-C irradiation.
(B) CldU/IdU ratios after S1-modified DNA fibre assay in cells treated with 5 J/m^2 UV-C or mock-treated as in (A), in presence of nonT or PrimPol siRNA.
(C) Percentages of cells with >5 RAD51 foci after release from 5 J/m^2 UV for the times indicated, in presence of nonT or PrimPol siRNA. n=3
(D) Percentages of cells with >5 RAD51 foci after treatment with 50 nM 4-NQO for the times indicated, in presence of nonT or PrimPol siRNA. n=3
(E) Percentages of cells with >5 RAD51 foci after treatment with 2 mM HU for 24 h, in presence of nonT or PrimPol siRNA. n=3
(F) Percentages of EdU positive cells with >10 RAD51 foci after release from 2 Gy IR for the time indicated, in presence of nonT or PrimPol siRNA. n=3.
The means and SEM (bars) of at least three independent experiments are shown. Asterisks indicate p-values (Mann-Whitney for B; student's t-test for C, D, E, F, * $p < 0.05$, ** $p < 0.01$, *** $p < 0.001$).

Figure 6. PrimPol is required for homologous recombination induced by bulky adducts.
(A) Relative recombination frequencies in SW480SN.3 cells induced by BPDE. Cells were treated with 50 nM BPDE for 20 min. n=4 (nonT solvent n=3)

(B) Colony survival assay of U2OS cells after 20 min treatment with BPDE at the indicated concentrations in presence of nonT, PrimPol or RAD51 siRNA. n=4 (RAD51 siRNA n=3)
(C) Strategy for detection of SCEs and representative picture of metaphase spreads in response to 50 nM BPDE.
(D) SCE formation in U2OS cells after treatment with 50 nM BPDE or solvent in presence of nonT or PrimPol siRNA.
(E) SCE formation in U2OS cells after treatment with 50 nM 4-NQO for 48 h in presence of nonT or PrimPol siRNA.
(F) Model of recombination at bulky DNA adducts. Left: In presence of PrimPol, re-priming creates gaps that are resected for RAD51 foci formation and recombination repair. Right: In absence of PrimPol, bulky DNA adducts are either bypassed by TLS or alternatively, stalled forks are stabilised by fork regression and potential rescue upon convergence with another fork.
The means and SEM (bars) of at least three independent experiments are shown. Asterisks indicate p-values (one-way ANOVA for A, B; Mann-Whitney for D, E, * $p < 0.05$, ** $p < 0.01$, *** $p < 0.001$).

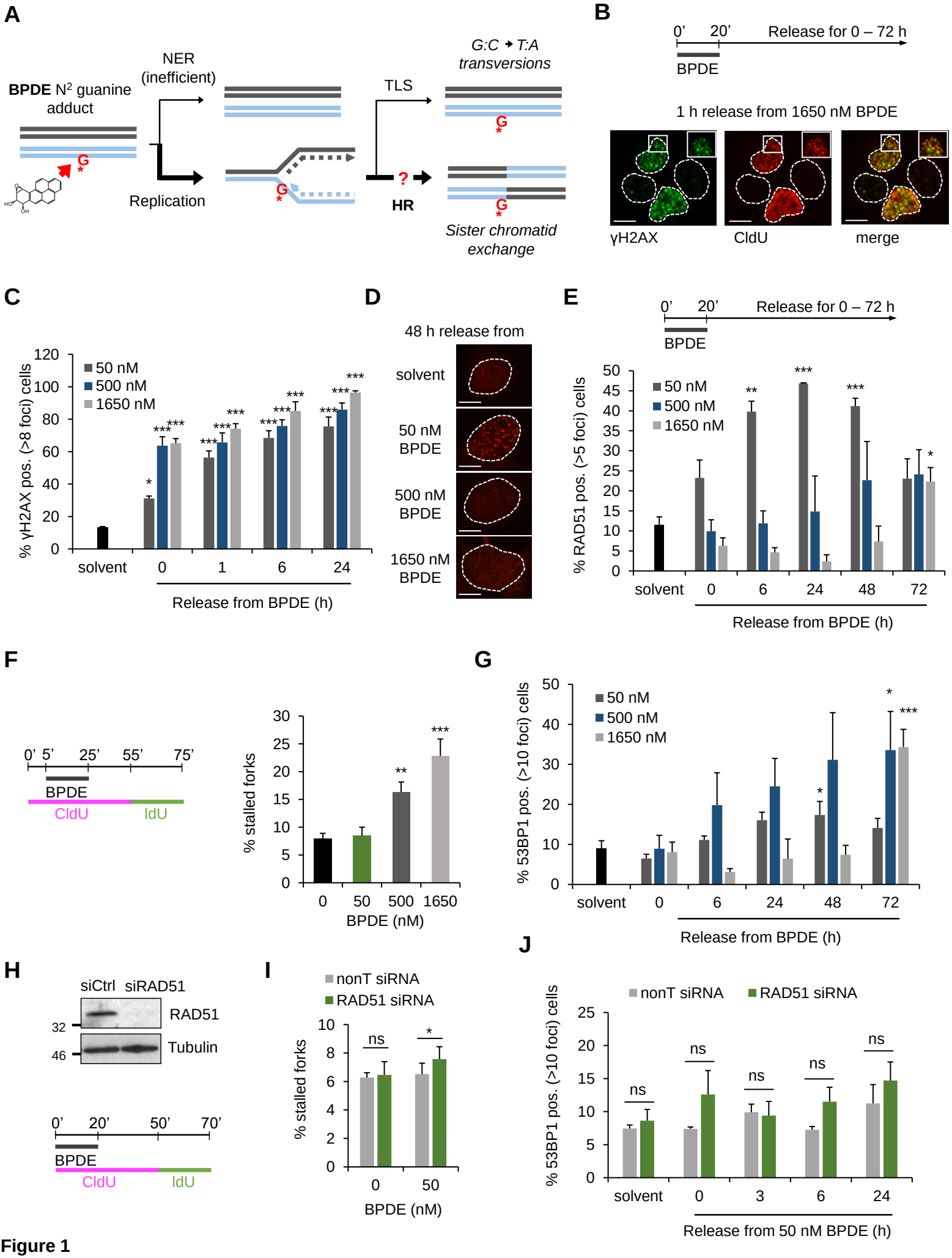
A
BPDE N2 guanine adduct
NER (inefficient)
Replication
TLS
HR
G:C → T:A transversions
Sister chromatid exchange
B
0' 20' Release for 0 – 72 h
BPDE
1 h release from 1650 nM BPDE
γH2AX
CldU
merge
C
% γH2AX pos. (>8 foci) cells
50 nM
500 nM
1650 nM
solvent
Release from BPDE (h)
D
48 h release from
solvent
50 nM BPDE
500 nM BPDE
1650 nM BPDE
E
0' 20' Release for 0 – 72 h
BPDE
% RAD51 pos. (>5 foci) cells
Release from BPDE (h)
F
0' 5' 25' 55' 75'
BPDE
CldU
IdU
% stalled forks
BPDE (nM)
G
% 53BP1 pos. (>10 foci) cells
Release from BPDE (h)
H
siCtrl siRAD51
RAD51
Tubulin
0' 20' 50' 70'
BPDE
CldU
IdU
I
nonT siRNA
RAD51 siRNA
% stalled forks
BPDE (nM)
J
nonT siRNA
RAD51 siRNA
% 53BP1 pos. (>10 foci) cells
Release from 50 nM BPDE (h)

Figure 1

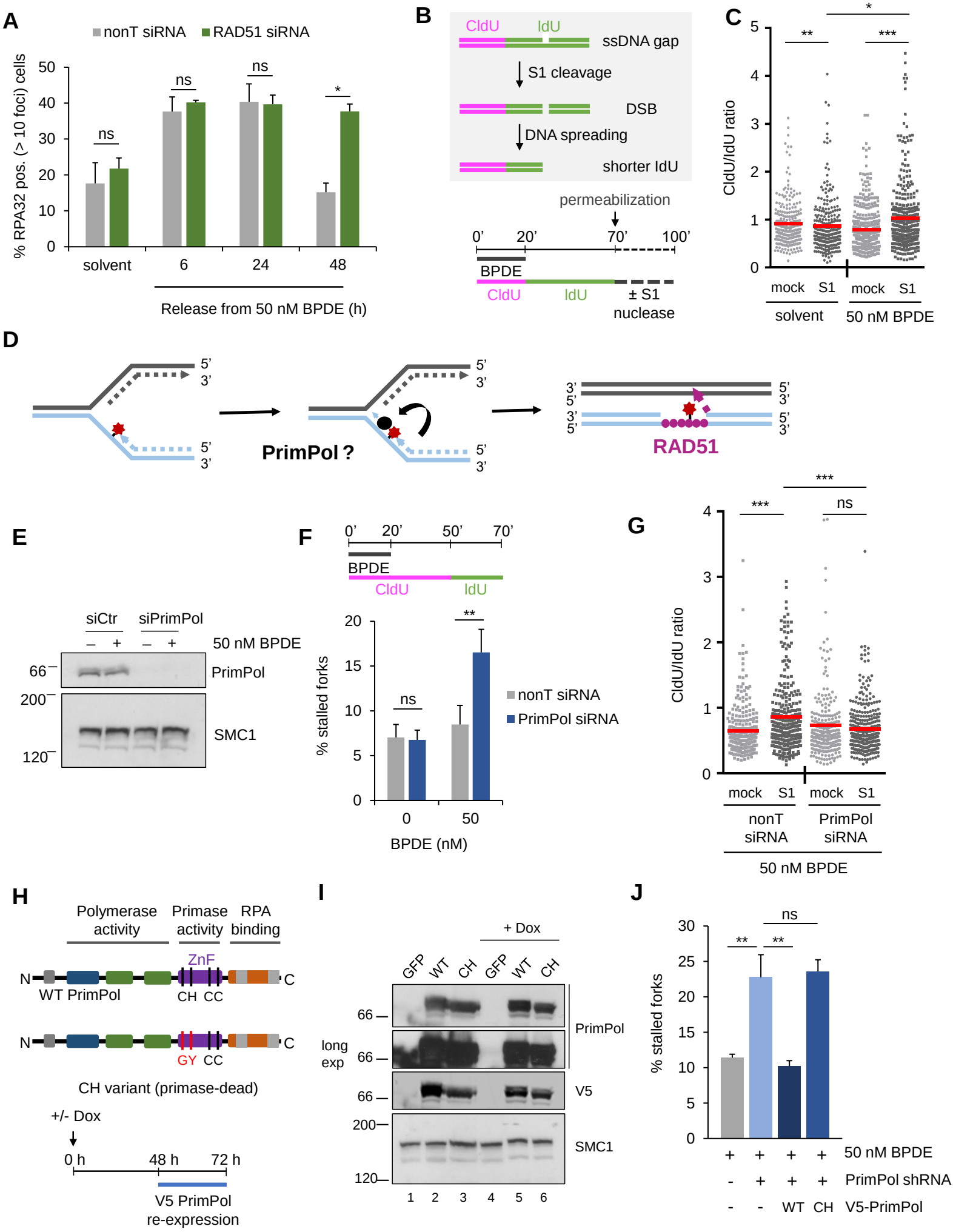
A
nonT siRNA
RAD51 siRNA
% RPA32 pos. (> 10 foci) cells
ns
ns
ns
*
solvent
6
24
48
Release from 50 nM BPDE (h)
B
CldU
IdU
ssDNA gap
S1 cleavage
DSB
DNA spreading
shorter IdU
permeabilization
0'
20'
70'
100'
BPDE
CldU
IdU
± S1 nuclease
C
CldU/IdU ratio
mock
S1
mock
S1
solvent
50 nM BPDE
D
5'
3'
PrimPol ?
RAD51
E
siCtr
siPrimPol
50 nM BPDE
PrimPol
SMC1
66
200
120
F
0'
20'
50'
70'
BPDE
CldU
IdU
% stalled forks
nonT siRNA
PrimPol siRNA
ns
**
BPDE (nM)
G
CldU/IdU ratio
***
***
ns
mock
S1
mock
S1
nonT siRNA
PrimPol siRNA
50 nM BPDE
H
Polymerase activity
Primase activity
RPA binding
ZnF
N
C
WT PrimPol
CH
CC
GY
CC
CH variant (primase-dead)
+/- Dox
0 h
48 h
72 h
V5 PrimPol re-expression
I
+ Dox
GFP
WT
CH
GFP
WT
CH
66
long exp
66
66
200
120
PrimPol
V5
SMC1
1
2
3
4
5
6
J
% stalled forks
ns
**
**
50 nM BPDE
PrimPol shRNA
V5-PrimPol
WT
CH

Figure 2

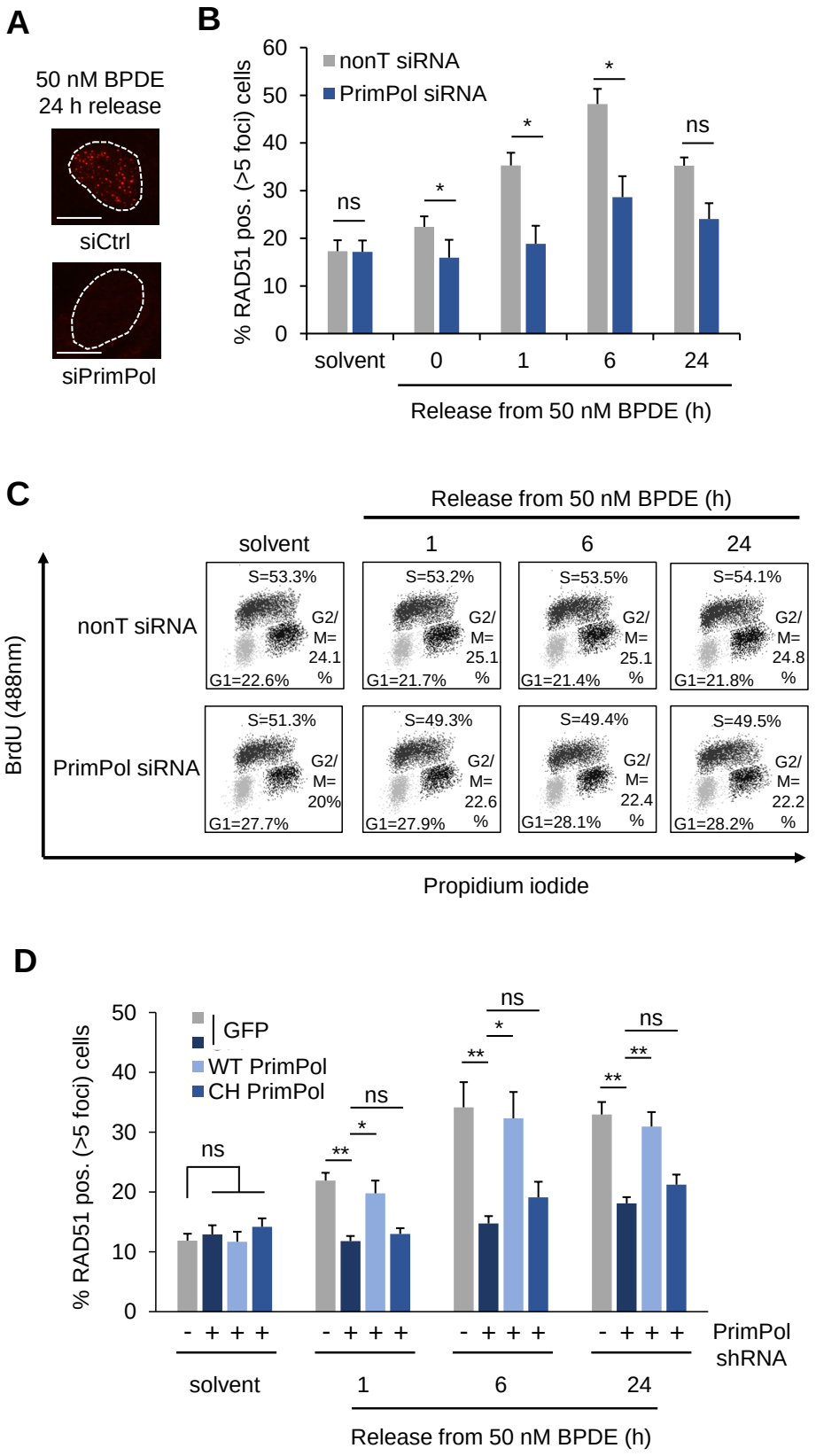
A
50 nM BPDE
24 h release
siCtrl
siPrimPol
B
nonT siRNA
PrimPol siRNA
% RAD51 pos. (>5 foci) cells
ns
*
*
*
ns
solvent
0
1
6
24
Release from 50 nM BPDE (h)
C
Release from 50 nM BPDE (h)
solvent
1
6
24
nonT siRNA
PrimPol siRNA
BrdU (488nm)
S=53.3%
G2/M= 24.1 %
G1=22.6%
S=53.2%
G2/M= 25.1 %
G1=21.7%
S=53.5%
G2/M= 25.1 %
G1=21.4%
S=54.1%
G2/M= 24.8 %
G1=21.8%
S=51.3%
G2/M= 20%
G1=27.7%
S=49.3%
G2/M= 22.6 %
G1=27.9%
S=49.4%
G2/M= 22.4 %
G1=28.1%
S=49.5%
G2/M= 22.2 %
G1=28.2%
Propidium iodide
D
GFP
WT PrimPol
CH PrimPol
% RAD51 pos. (>5 foci) cells
PrimPol shRNA
solvent
1
6
24
Release from 50 nM BPDE (h)

Figure 3

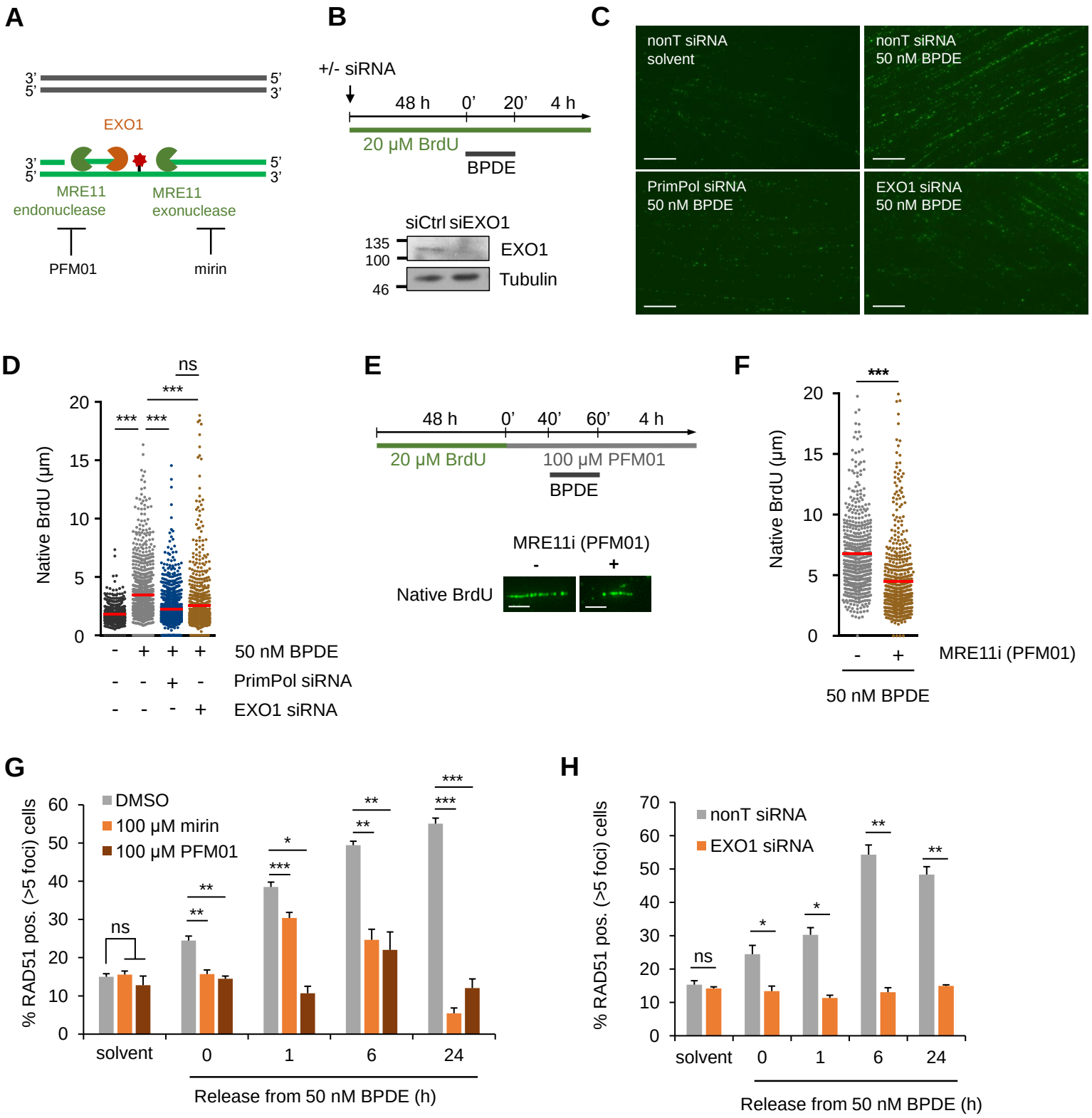
A
3'
5'
5'
3'
EXO1
MRE11
endonuclease
MRE11
exonuclease
PFM01
mirin
B
+/- siRNA
48 h
0'
20'
4 h
20 µM BrdU
BPDE
siCtrl siEXO1
135
100
46
EXO1
Tubulin
C
nonT siRNA
solvent
nonT siRNA
50 nM BPDE
PrimPol siRNA
50 nM BPDE
EXO1 siRNA
50 nM BPDE
D
Native BrdU (µm)
ns
***
50 nM BPDE
PrimPol siRNA
EXO1 siRNA
E
48 h
0'
40'
60'
4 h
20 µM BrdU
100 µM PFM01
BPDE
MRE11i (PFM01)
Native BrdU
F
Native BrdU (µm)
MRE11i (PFM01)
50 nM BPDE
G
% RAD51 pos. (>5 foci) cells
DMSO
100 µM mirin
100 µM PFM01
solvent
Release from 50 nM BPDE (h)
H
% RAD51 pos. (>5 foci) cells
nonT siRNA
EXO1 siRNA
solvent
Release from 50 nM BPDE (h)

Figure 4

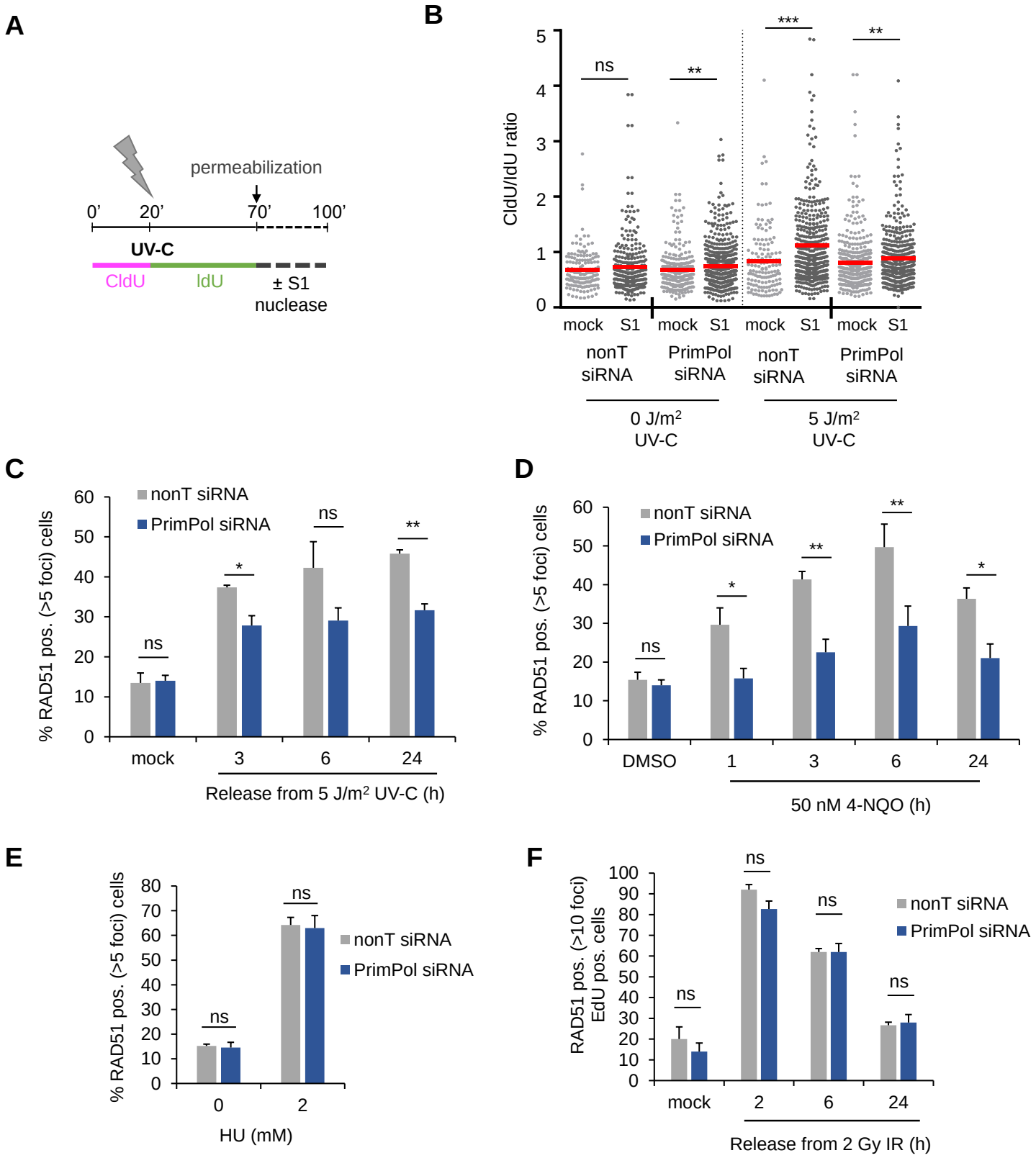
A
permeabilization
0'
20'
70'
100'
UV-C
CldU
IdU
± S1
nuclease
B
CldU/IdU ratio
ns
**
***
**
mock
S1
mock
S1
mock
S1
mock
S1
nonT
siRNA
PrimPol
siRNA
nonT
siRNA
PrimPol
siRNA
0 J/m2
UV-C
5 J/m2
UV-C
C
% RAD51 pos. (>5 foci) cells
nonT siRNA
PrimPol siRNA
ns
*
ns
**
mock
3
6
24
Release from 5 J/m2 UV-C (h)
D
% RAD51 pos. (>5 foci) cells
nonT siRNA
PrimPol siRNA
ns
*
**
**
*
DMSO
1
3
6
24
50 nM 4-NQO (h)
E
% RAD51 pos. (>5 foci) cells
nonT siRNA
PrimPol siRNA
ns
ns
0
2
HU (mM)
F
RAD51 pos. (>10 foci)
EdU pos. cells
nonT siRNA
PrimPol siRNA
ns
ns
ns
ns
mock
2
6
24
Release from 2 Gy IR (h)

Figure 5

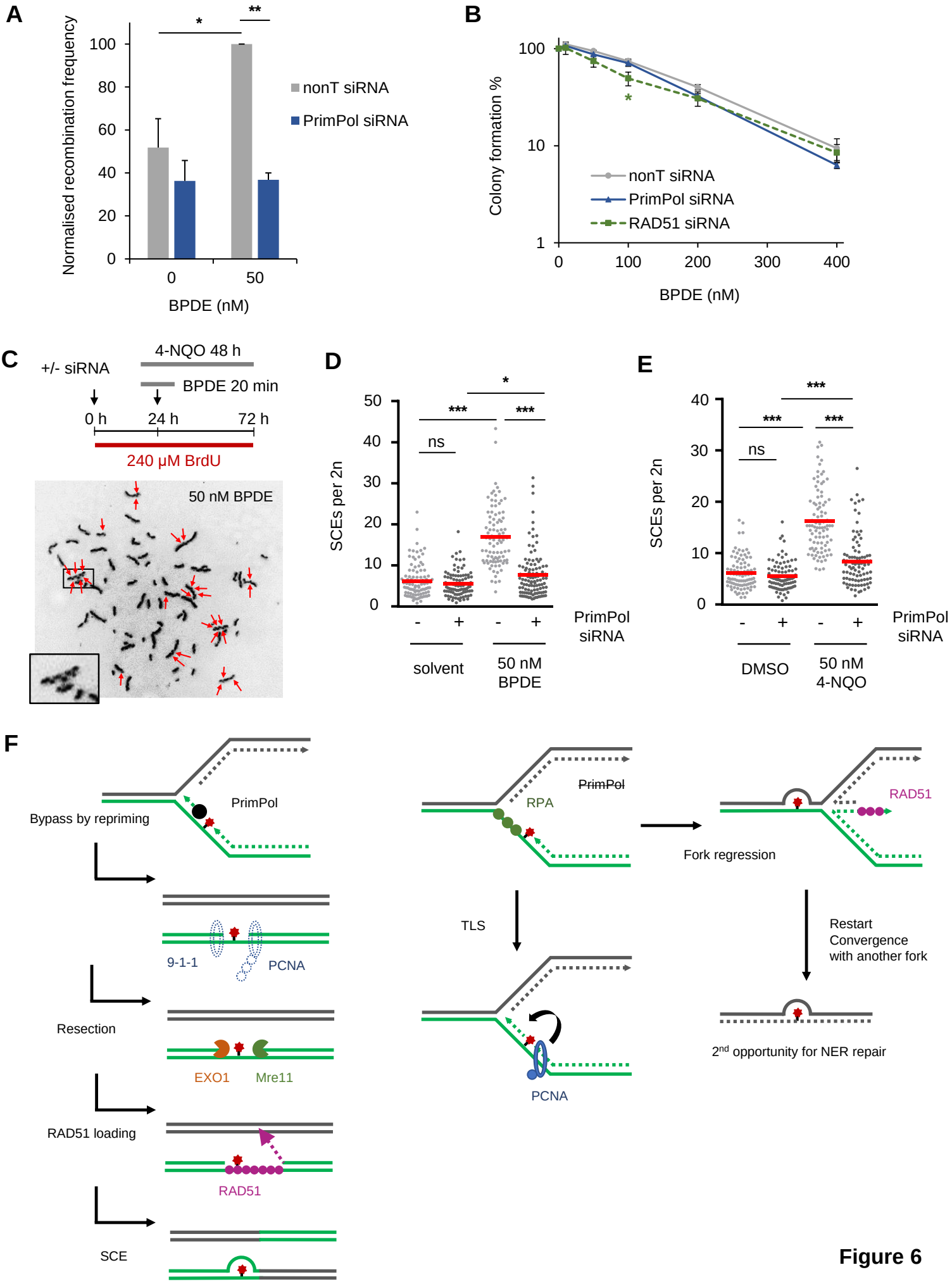
A
Normalised recombination frequency
100
80
60
40
20
0
*
**
nonT siRNA
PrimPol siRNA
0
50
BPDE (nM)
B
Colony formation %
100
10
1
*
nonT siRNA
PrimPol siRNA
RAD51 siRNA
0
100
200
300
400
BPDE (nM)
C
+/- siRNA
4-NQO 48 h
BPDE 20 min
0 h
24 h
72 h
240 µM BrdU
50 nM BPDE
D
SCEs per 2n
50
40
30
20
10
0
*
***
***
ns
-
+
-
+
PrimPol siRNA
solvent
50 nM BPDE
E
SCEs per 2n
40
30
20
10
0
***
***
***
ns
-
+
-
+
PrimPol siRNA
DMSO
50 nM 4-NQO
F
Bypass by repriming
PrimPol
9-1-1
PCNA
Resection
EXO1
Mre11
RAD51 loading
RAD51
SCE
PrimPol
RPA
TLS
PCNA
Fork regression
RAD51
Restart Convergence with another fork
2nd opportunity for NER repair

Figure 6